Cu,Zn-based catalysts for methanol synthesis: On the effect of calcination conditions and the part of residual carbonates.

Julia Schumann[a], Andrey Tarasov[a], Nygil Thomas[a,1], Robert Schlögl[a,b], Malte Behrens[a,2]

[a]Department of Inorganic Chemistry
Fritz-Haber-Institut der Max-Planck-Gesellschaft
Faradayweg 4-6, 14195 Berlin (Germany)
Fax: (+49) 30-8413-4401
E-mail: schumann@fhi-berlin.mpg.de
tarasov@fhi-berlin.mpg.de
nygill@gmail.com
acsek@fhi-berlin.mpg.de
malte.behrens@uni-due.de

[b]Department of Heterogeneous Reactions
Max-Planck-Institut für Chemische Energiekonversion
Stiftstrasse 34–36, 45470 Mülheim an der Ruhr (Germany)

Present addresses

[1] Postgraduate and Research Department of Chemistry
Nirmalagiri College, Nirmalagiri, Kannur, Kerala (India)

[2] University of Duisburg-Essen
Faculty of Chemistry and Center for Nanointegration Duisburg-Essen (CENIDE)
Universitätsstrasse 7, 45141 Essen (Germany)
Tel: (+49) 201/183-3684

Corresponding author

Andrey Tarasov: tarasov@fhi-berlin.mpg.de

Abstract

Cu/Zn based catalysts for methanol synthesis derived from zincian malachite and aurichalcite precursor phases were investigated. The decomposition process of the different hydroxy-carbonates to yield the carbonate modified metal oxides (calcined precursor) was studied in detail on the basis of the results of nonisothermal kinetics modeling. It was possible to obtain different amounts of the so-called high temperature carbonate (HT-CO_3) in the calcined material after calcination at the same temperature by varying the mass transfer conditions, which resulted in differences in crystallinity, IR spectra and decomposition profile. Large amounts of HT-CO_3 in the calcined material seem to be detrimental, whereas only a small fraction is beneficial and effects phase stability.

Keywords

zincian malachite, aurichalcite, methanol synthesis, thermal analysis, deactivation

1. Introduction

Two of the most relevant precursor phases for the preparation of Cu,Zn based catalysts are zincian malachite [$(Cu,Zn)_2CO_3(OH)_2$] (ZM) and aurichalcite [$(Cu,Zn)_5(CO_3)_2(OH)_6$] (AU) [1]. Numerous studies investigated the influence of parameters of the precursor formation as ageing, pH value, temperature and elemental composition [2-7]. The activity of the final catalyst strongly depends on the properties fixed during those early stages of the catalyst preparation. Although it is known that wrong conditions can ruin a “good” precursor phase [8], relatively few systematic studies have been performed about the calcination step of the catalyst synthesis [9]. Typically synthetic mixed hydroxy-carbonate phases decompose in two main steps, a first one with simultaneous evolution of H_2O and CO_2 and a second one at higher temperature with evolution of CO_2 only. The intermediate is called anion modified mixed metal oxide[4] or high temperature carbonate (HT-CO_3) [2]. Although the occurrence of this high temperature stable carbonate in the precursor phase is said to be beneficial for the Cu dispersion in the final catalyst [10], detailed investigations about the calcination process and understanding of the role of HT-CO_3 for catalysis are still lacking.

The influence of self-generated gaseous products on the kinetics and mechanism of thermal decomposition of synthetic malachite, $Cu_2CO_3(OH)_2$, was first studied by Koga and co-workers [11]. In water containing atmosphere the carbonate decomposes more rapidly and already at lower temperatures [9, 12]. The evolved water during decomposition promotes the crystallization of CuO. This effect was also observed by Fujita et al. [9, 13] who studied the influence of the heating rate during calcination on the methanol formation rate over the resulting catalysts. It was demonstrated that calcination at mild heating rates results in better dispersed CuO and ZnO, thus preventing

aggregation of oxides and leading to higher dispersion of metal particles in the reduced catalyst. A detailed kinetic analysis of the decomposition process of ZM and AU was published by our group recently [12]. We showed that the decomposition of the HT-CO_3 is significantly influenced by the transport conditions of the evolved water.

The aim of this study is to investigate the influence of the calcination parameters on the properties and catalytic performance of catalysts derived from both ZM and AU precursors, which differ in their Cu/Zn-ratio. Results of thermokinetic studies on binary Cu/Zn samples in a thermobalance as well as application on larger batch calcination experiments are presented. With the knowledge of the formal calcination kinetics, the decomposition rate as well as the amount of the reaction products can be controlled. Two series of calcined samples were prepared, from both ZM and AU precursor. We varied the amount of the residual HT-CO_3 by controlling water transfer conditions during the calcination. The resulting materials have been characterized in detail by XRD, TG analysis and IR spectroscopy and the activity of the final catalysts have been tested in methanol synthesis. The influence of intermediate HT-CO_3 on the catalyst activity in methanol synthesis and the effect of the calcination rate on the development of surface area of the binary precursors were revealed.

2. Experimental

2.1. Sample preparation

Cu/Zn precursors were prepared by pH-controlled co-precipitation [14] in an automated reactor (LabMax from Mettler-Toledo). The proper amount of $Cu(NO_3)_2{\cdot}3H_2O$ and $Zn(NO_3)_2 \cdot 6H_2O$ was dissolved in Millipore water and 15 ml of concentrated HNO_3 to obtain 600 ml of a 1 M solution of the metal salts. This solution was added to the reactor containing 400 ml of water at a constant rate of 20 ml/min. The proper amount of Na_2CO_3 solution (1.6 M) was automatically added to keep the pH constant at 6.5. The precipitation temperature was 338 K. Precipitation was followed by ageing for 1 h (338 K, pH=6.5), once the turbidity started to increase. The solid was then filter-collected and washed several times by re-dispersion in water until the conductivity of the washing medium was below 0.5 mS/cm. Approximately 40 g of the solid hydroxy-carbonate precursors were obtained by spray drying. The molar Cu:Zn ratios were 80:20 and 40:60 resulting in the ZM and AU precursor materials with the nominal chemical formulae $(Cu_xZn_{1-x}(CO_3)(OH)_2$ (x=0.8) and $(Cu_xZn_{1-x})_5(CO_3)_2(OH)_6$, (x=0.4), respectively. XRD confirmed that both precursor materials were phase pure. The original XRD pattern and the results of Rietveld refinement are presented elsewhere [12].

The samples were calcined in a rotating furnace, (turn number of 3 per min, tube diameter 40 mm and length of sample bed 300 mm) with a flow of 100 ml/min in 20% O_2 in Ar. 0.75 g of the precursor

powder were calcined at a maximum temperature of 603 K and a dwell time of 180 min, the heating rates were varied between 0.1 and 2 K min^{-1}. The sample without residual high temperature carbonate was synthetized under static conditions with heating rate of 2 Kpm.

2.2. Characterization Methods

X-ray diffraction (XRD) data were collected using a STOE STADI P transmission diffractometer equipped with a primary focusing Ge monochromator (Cu $K_{\alpha 1}$ radiation) and a linear position sensitive detector (moving mode, step size 0.5 °, counting time 30 s/step). The samples were mounted in the form of a clamped sandwich of small amounts of powder fixed with a small amount of grease between two layers of thin polyacetate film. The phase composition was determined by full pattern refinement in the 2θ range 4-80 ° according to the Rietveld method using the TOPAS software [15] and crystal structure data from the ICSD database. Summarized refinement parameters are displayed in the Supplementary Information (SI).

Thermogravimetric analysis (TG/DSC) was performed on a Netzsch STA449 Jupiter thermoanalyzer Around 10-15mg of the sample was positioned in corundum 85µl crucible without lid and heated with 10 K min^{-1} in 100Nml/min 21% O_2 in Ar. Prior the measurement, the system was purged with the reaction gas for 30 min. Evolution of the gas phase during reaction was monitored with a quadrupole mass spectrometer (Pfeiffer, QMS200 Omnistar). The kinetic data obtained in the TG experiments were processed using Netzsch software and are presented elsewhere [12]. The Thermokinetics program package was used for processing kinetic dependences and for component kinetic analysis. The NETZSCH Procedure is described in [16, 17].

IR spectra of precursors and calcined samples were recorded using an ATR Vario 670 spectrometer, equipped with an MCT detector and diamond as ATR crystal. No pretreatment of the powdered samples was performed. The aperture was set to 0.5 cm^{-1} and the resolution was 4 cm^{-1}. Spectra were recorded using 64 scans.

Specific surface areas were determined by N_2 physisorption using the BET method [18] in a Quantachrome Autosorb-1 machine. Prior to analysis, the samples were degassed for 2 h at 353 K. The mesopore size distribution and pore volume were calculated according to Barrett, Joyner and Halenda modified Kelvin equation [19]. N_2O chemisorption capacity was determined using reactive frontal chromatography (RFC) [20]. Approx. 100 mg of calcined sample (100-200 µm particle size) was placed in a fixed bed reactor. After in-situ reduction (6 K min^{-1}, 250°C, 30min hold, 80Nml/min 5%H_2 in Ar), the sample was cooled down in the reducing gas to room temperature, purged with He and then switched to 10 mL/min of a 1% N_2O in He mixture. The N_2O chemisorption capacity and

resulting Cu surface area (Cu-SA_{N2O}) were calculated from the MS signal of the N_2 trace (m/z =28). Apparent Cu-SA_{N2O} were calculated assuming a stoichiometry of N_2: Cu 1:2, according to the surface reaction $N_2O + 2\ Cu \rightarrow Cu_2O + N_2$ and an average surface density of $1{,}47\times10^{19}$ Cu-atoms per m^2. The values are normalized to the weight of calcined precursor put into the reactor. The accuracy of the measurement is estimated with ± 1 $m^2\ g_{calc}^{-1}$.

2.3 Catalytic measurements

Methanol synthesis from syngas was tested in a fixed bed flow reactor. 50 mg (100-200 µm particle diameter, diluted with 0.7 g of SiO_2) were loaded into a 6 mm inner diameter stainless steel reactor tube using a bed volume of 1.7 mL, which resulted in a GHSV of 3500 h^{-1}. The calcined precursor was reduced at 523 K (1 K min^{-1}) for 1.5 hours in 20 % H2 in Ar to obtain the active catalyst. Upon completion of the reduction, the reactor was cooled to 503 K, a syngas mixture with a composition of 6 % CO, 8 % CO_2, 59 % H_2 and balance Ar was introduced into the reactor, and the pressure was raised to 30 bars. Online analysis of products was performed with a gas chromatograph (Agilent 7890A). Methanol synthesis was performed under differential conditions (<4% conversion). Turn over frequency was calculated using N_2O capacity of the samples determined by N_2O RFC method.

3. Results and Discussion

3.1. Constant mass loss calcination and its influence on the porosity

Consideration of the calcination kinetics allows controlling the decomposition rate of the hydroxy-carbonate precursor. It was demonstrated in [21] that thermal carbonization of polymer materials with constant mass loss rate has a beneficial effect on BET specific leading to a narrower pore size distribution compared to samples prepared using constant heating rate. Ruland et al. and Busser [22, 23] studied the influence of the constant rate reduction and calcination on the specific copper surface area and the catalytic performance of a ternary $Cu/ZnO/Al_2O_3$ catalyst applied in methanol synthesis. No significant catalytic effect of the milder reduction/calcination conditions was observed compared with a slow linear heating ramp. It is worth noting that constant rate experiments are performed with respect to one single gaseous component which evolution or consumption rate is kept constant during the reaction whereas in constant mass loss rate analysis the mass change rate of the solid product remains invariable. This implies precise control over the rate of the whole process, which is the complex interplay of several gas-solid reactions. In constant mass loss rate calcination the evolution of all gaseous products (H_2O, CO_2) is controlled with respect to formation rate of the solid oxide mixture. This approach might have a more pronounced effect on porosity or activity. Reading and Dollimore [24] examined thermal decomposition of synthetic malachite by

means of constant rate thermal analysis (CRTA). The $Cu_2CO_3(OH)_2$ sample was thermally decomposed under flowing nitrogen maintaining a weight loss rate of 0.06 wt.%/min with a maximum temperature reached at 603 K. It was shown that there is a non-linear relationship between the extent of the decomposition reaction and the BET surface area. The surface area increases to the reaction extent of 92% (26.4% weight loss). A drop of the surface area is observed upon subsequent heating to final temperature. The authors suggested that water loss is associated with a greater surface area increase than carbon dioxide.

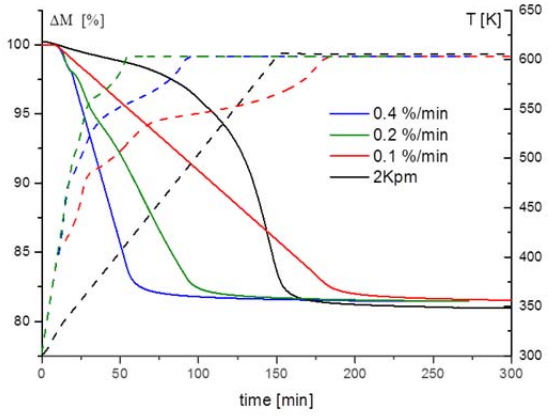

Figure 1: experimental TG curves of AU precursor with constant heating rate (black curve) and constant mass loss rate (blue, green, red curve). Dashed line indicates the temperature program. Control over mass loss is established due to verified parameters of nonisothermal decomposition kinetics.

Based on the determined formal decomposition mechanism and thermokinetic parameters [12] several temperature programs were calculated enabling calcination of AU with the constant mass loss rate (Figure 1). Table 1 summarizes the BET-SA values of the samples calcined with constant mass loss rate and of a conventionally (with constant heating rate) calcined AU sample. The maximum reached temperature was 603 K, with holding time of 3 h. A decrease in the BET surface was observed with the higher heating rates. The pore size distribution of the calcined material did not undergo crucial changes within the parameter space covered (Figure S1 in SI), unlike demonstrated for other systems [21]. This result indicated that the properties of the calcined materials were stronger depending on the final temperature rather than on the heating rate what is in good agreement with [24]. Analogous behaviour was observed for the pure ZM precursor.

Table 1: BET-SA of the calcined AU precursor

Calcination program	BET-SA, $m^2\ g_{calc}^{-1}$
2Kpm, 330°C, 3hrs	97
0.1wt%/min, 330°C, 3hrs	91
0.2wt%/min, 330°C, 3hrs	89
0.4wt%/min, 330°C, 3hrs	76

These experiments were performed to find the correlation of mass loss rate and the resulting BET surface area of the calcined sample. Unfortunately due to absence of the distinct effect on the pore size distribution and experience of other research groups [22, 23] the samples calcined at constant mass loss rate were not further considered for methanol synthesis tests.

3.2. Calcination series of binary precursors

The typical calcination temperatures around 600 K would favor the formation of HT-CO_3 for both precursor structures. Further increase of calcination temperature may cause a decrease of the surface area and segregation and sintering of the metal oxides. High temperature carbonate (HT-CO_3) has been considered as a possible reason for the superior catalytic activity of methanol synthesis catalysts prepared by the co-precipitation route via basic carbonate precursors, but its exact role for the catalytic activity remained unclear [10, 25]. In order to gain better understanding of the HT-CO_3 we prepared two series of catalysts from AU and ZM by variation of the calcination conditions.

Results of formal kinetic analysis of our previous study [12] enabled us to predict the amount of the reaction products under different calcination conditions. Figure 2 illustrates the changes in solid components of the reaction upon decomposition of ZM precursor at 2 Kpm. Concentration in Figure 2 stands for the amount of the corresponding species of the substance in the solid product of reaction. MO(1) and MO(2) are oxides obtained via two competitive decomposition routes. Chemically they are identical but they have different microstructure due to other formation path [12].

The high temperature carbonate starts to accumulate from 510 K and completely decomposes at 740 K. The total amount of the HT-CO_3 might be regulated either by varying the maximum calcination temperature or modifying the product transfer conditions e.g. by changing the heating rate or gas flow.

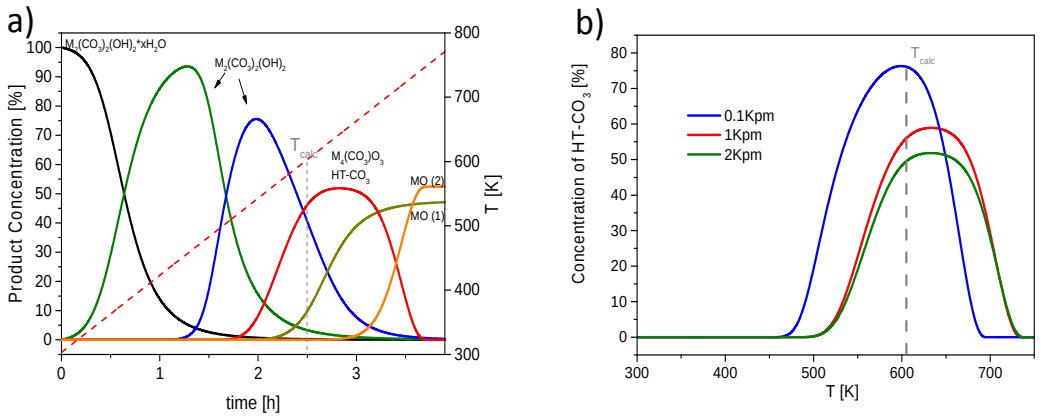

Figure 2: a) Component kinetic analysis of ZM decomposition at 2 Kpm. b) Kinetic Simulation of residual carbonate (HT-CO_3) evolution at different heating rates. Based on the results of the thermokinetic calculation performed in [12] the evolution of solid products with temperature is assessed.

Figure 2b depicts the simulated evolution of the HT-CO_3 concentration in solid products of ZM decomposition at different heating rates. By increasing the heating rate, more water accumulates in the atmosphere above the sample as the result of faster decomposition of the sample and H_2O cannot be purged out fast enough. The amount of water in the atmosphere during calcination crucially influences the decomposition kinetics of the hydroxy carbonate by promoting the decomposition of the HT-CO_3 and the crystallization of the metal oxides CuO and ZnO in agreement with results from the literature [9, 11]. This effect was additionally demonstrated with experiments where H_2O was introduced artificially during the calcination process [9, 12].

It should be noted that great care should be taken by upscaling the results of kinetic analysis for massive calcination ovens and larger catalyst batches. Since the mass and heat transfer conditions in the thermobalance are optimized for the TG experiment and very crucial for the process kinetics it remains difficult to impose identical conditions on the calcination furnace with other design and geometrical parameters. Taking into consideration the simulated data and conditions set in the thermobalance both precursor series were calcined in a rotating furnace with different heating rates between 0.1 and 2 Kpm and a reasonable small batch size of < 1 g. Rotation of the calcination tube was applied in order to further reduce the mass transfer limitation.

3.3. Characterization of the calcined precursors

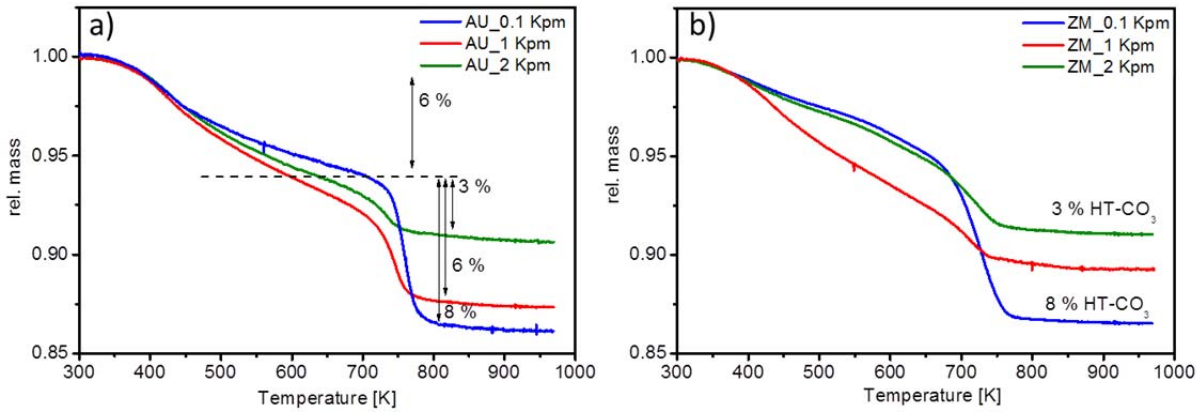

Figure 3: TG curves at 10 Kpm of a) calcined AU and b) calcined ZM samples prepared using different heating rates. Heating rate variation enables control of HT-CO_3 amount in the calcined sample.

TG investigations of three of the calcined samples of each series revealed, that catalysts heated with different heating rates contain different amounts of HT-CO_3 after calcination (see Figure 3) and are thus suited to study the role of HT-CO_3 without too many other factors interfering into the data interpretation. Due to relatively high surface area the samples also tend to adsorb moisture and at less extent CO_2 after exposure to air. As proved with the subsequent TG-MS experiments of the calcined samples the weight loos preceding the high temperature carbonate decomposition is mainly ascribed to water (Fig S2). After a weight loss at low temperature due to desorption of moisture from the calcined precursors, the HT-CO_3 decomposition is observed at temperatures around 700 K, i.e. at similar values as predicted in Figure 2b. The samples calcined with the slowest ramp of 0.1 Kpm contain the highest amount of HT-CO_3, whose decomposition led to a mass loss of about 8 %, which is close to the theoretical maximum [12]. Increasing the heating ramp up to 1 Kpm led only to small changes of the residual fraction of HT-CO_3. Only the samples calcined with the 2 Kpm ramp contained less HT-CO_3, corresponding to a mass loss of about 3%. Samples calcined in static environment basically do not contain any strongly bound carbonates, which are released at high temperature, because the accumulating evolved gases led to a reduction of the decomposition temperature. Slow heating ramps and small amounts of sample represent very dry conditions of calcination, leading to a correspondingly higher decomposition temperature of the carbonate.

This was further confirmed by XRD measurements (Figure 4). The samples with the highest heating rates were most crystalline in both series, with domain sizes of CuO or ZnO of around 3 nm (see Table S1 in SI). The samples of the ex-AU series with heating rates smaller 2 Kpm were nearly amorphous, with some weak features that cannot be ascribed to either ZnO or CuO (Figure 4a). Some very weak features around 11° and 30° 2 θ could be ascribed to originate from undecomposed

AU precursor. The samples derived from the ZM precursor on the other hand all displayed crystalline CuO in their diffraction pattern. The minor component ZnO is not crystalline (see Figure 4b). Only under harsher conditions, in static atmosphere, ZnO crystallized from the ZM phase. For both ZM and AU phases calcination under static atmosphere led to domain sizes of CuO and ZnO of 5-6 nm (see Table S1 in SI).

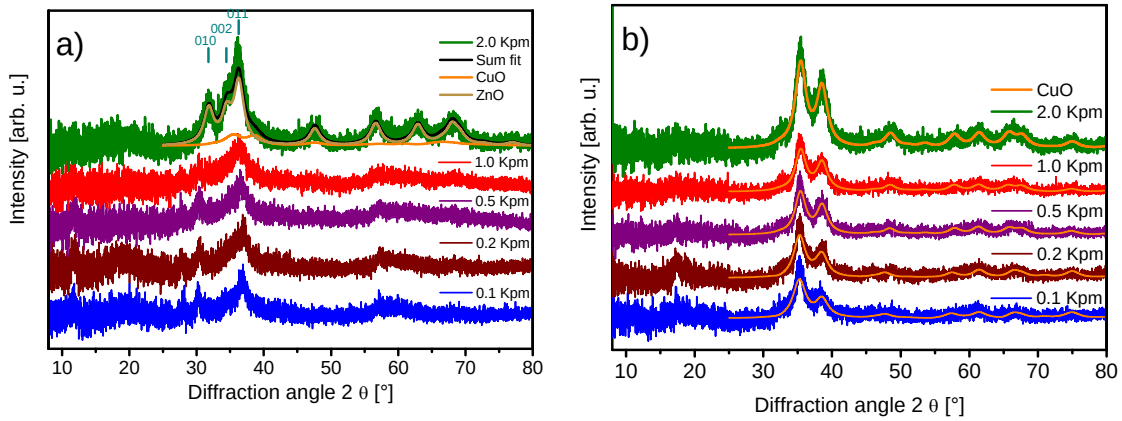

Figure 4: XRD pattern of a) AU sample series b) ZM samples calcined at 330°C for 3 h with different heating rates. The background of the pattern was subtracted and the pattern were vertically offset for clarity. The crystallinity grows with increasing heating rate.

IR spectra of the calcined samples showed bands in the carbonate vibration regions (displayed in Figure 5). The bands attributed to the M-OH bonds (500-1200cm^{-1}) [26] in the precursor have vanished. Comparison of the spectra of the calcined samples with those of the precursors showed some similarity of the remaining HT-CO_3 with features of the precursor, especially in the AU series. One should be noted that characteristic carbonate absorptions in range of 1300-1500 cm^{-1} is in a good agreement with IR spectra of CuZn mixed oxide (3600-1100 cm^{-1}) recorded at 140°C in vacuum with in-situ treatment at 250°C under vacuum for 70 hrs reported by Khassin et al. [27]. The vibration bands of the free CO_2 molecule ca. 2350 cm^{-1} are much weaker than carbonate stretching modes (1600-1300cm^{-1}) (SI Fig S3). The adsorbed water is present mostly as isolated molecule on the surface and not as OH groups within MO skeleton since the corresponding OH bands (500-1200cm^{-1}) are disappeared and the broad bands 3100-3600cm^{-1} are present (SI Fig S3) [28]. In that matter we neglect the influence of adsorbed CO_2 due to exposure to air on the relevant band regions. The four strong bands observed in AU precursor at 1558, 1507, 1406 and 1366 cm^{-1} (see Figure 5a), corresponding to the asymmetric C-O stretching mode ν_3 of carbonate, agreed very well with the data published in the literature [5, 25, 29]. In the calcined AU sample series 4 bands could still be

recognized. The large number of bands in the carbonate asymmetric stretching vibration region can be related to the 4 differently coordinated metal centers (octahedral, tetragonally elongated, tetrahedral and trigonal bipyramidal) present in the aurichalcite structure and to the symmetry reduction of the coordinated carbonate compared to the free carbonate ion (see also Figure 6 for comparison) [29]. Additionally, the splitting of the ν_3 band observed for AU indicates a symmetry reduction of the carbonate. The magnitude of the splitting indicates a monodentate coordination of the carbonate to the metal cation [30].

The ZM precursor also agreed reasonably well with the literature data [5, 25]. Two strong bands were observed at 1504 and 1383 cm^{-1} and a shoulder at 1427 cm^{-1} (Figure 5c), the smaller number of different bands correlating to the lower number of crystallographically different metal centres (2), both of them octahedrally coordinated with a tetragonal elongation. The calcined ZM samples exhibit only one very broad feature, consisting of 2-3 components with a smaller splitting than in the precursor (see Figure 5c). These findings suggest that in the calcined ZM samples, the carbonates resemble a lot like free carbonate ions, with a symmetric surrounding of the carbonate, whereas in the calcined AU samples the carbonate ions are more strongly bound via one oxygen atom in a monodentate fashion.

In the range between 1200 to 500 cm^{-1} deformation vibrations of OH and further carbonate bands appeared for the precursors (see Figure 5b and d). The strong and broad OH deformation bands of the precursors at 1032, 968 and 866 cm^{-1} for AU and 1101, 1049 and 865 cm^{-1} for ZM precursor all vanish after calcination, supporting the complete decomposition of the hydroxyl groups. In line with this conclusion, the special fingerprint feature for AU precursor, a M-OH band at 1208 cm^{-1}, also disappeared. Some weak bands remain that correspond to out-of-plane and asymmetric O-C-O bending modes of carbonate (ν_2 and ν_4). For the calcined AU series these correspond to a band at 703 and split band around 837 cm^{-1}. A third feature of the AU series at 1058 cm^{-1} can be attributed to a symmetric stretching vibration of carbonate (ν_1), which is theoretically expected for malachite samples at 1085 cm^{-1} according to literature [31]. The absence of the symmetric stretching vibration band in case of the calcined ZM samples further supports the assumption, that these carbonates are very weakly bound, in a symmetric environment inside the samples as it is the case for free carbonate-ions where this vibration is IR-inactive, due to the lack of dipole change during the vibration. The band at 820 cm^{-1} and below 650 cm^{-1} can be related to the bending modes ν_2 and ν_4. Below 600 cm^{-1} the rise of a broad feature was observed for both series, which could be attributed to the vibrations of the M-O skeleton, as published in literature [26].

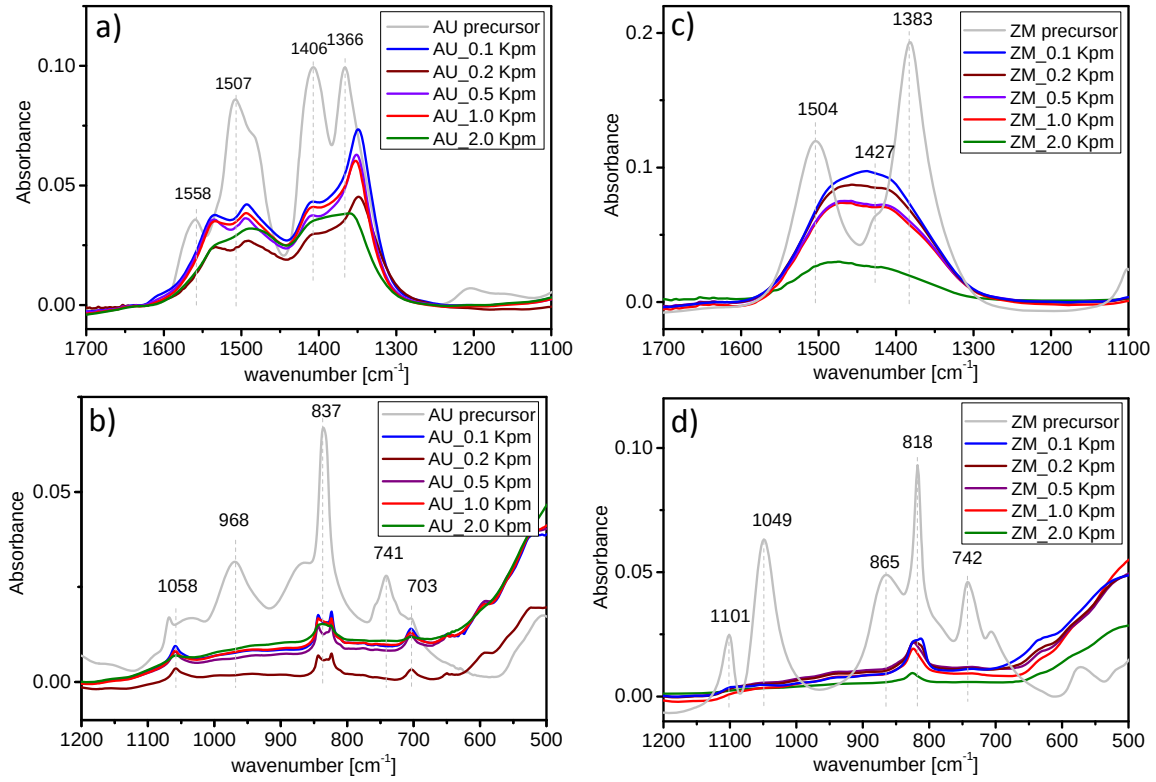

Figure 5: IR spectra of calcination series AU ((a) and b)) and ZM_((c) and d)) calcined at different heating rates.

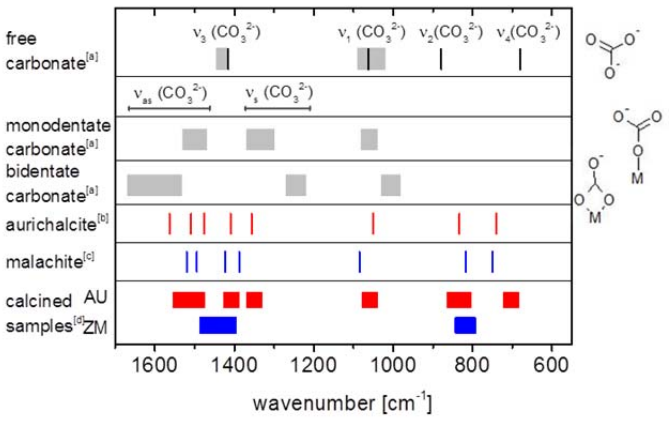

Figure 6: IR vibrational frequency correlation chart of different carbonate species on metal oxides. Literature values taken from [a] Ref. [30, 32] [b] Ref. [29] [c] Ref. [25] [d] values from this study. ZM calcined samples contain free carbonate species whereas monodentate coordinated carbonate persists in AU calcined samples along with free carbonates.

3.4. Catalyst activation

During catalyst activation, the calcined precursors are reduced by hydrogen to yield Cu/ZnO.

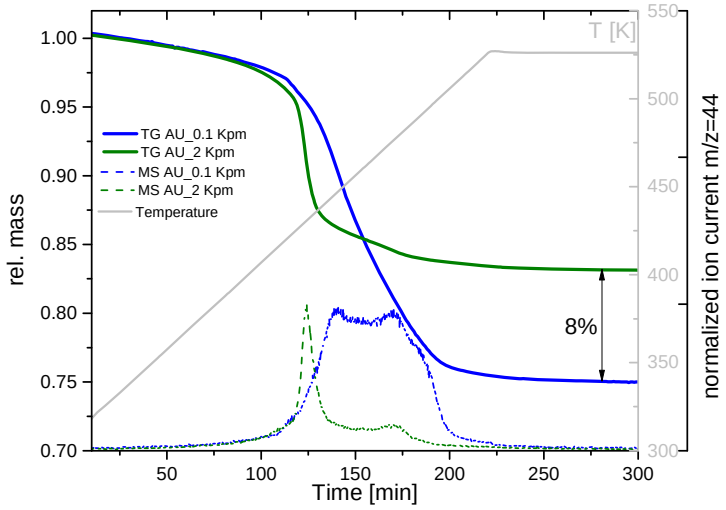

Figure 7 shows the mass loss and simultaneous carbon dioxide evolution of calcined precursors during reduction. Taking into consideration the strong overlapping effect of CuO reduction the mass loss difference of 8 % is in agreement with the difference in HT-CO_3 content, which is a strong indication that the carbonate decomposes under reducing conditions.

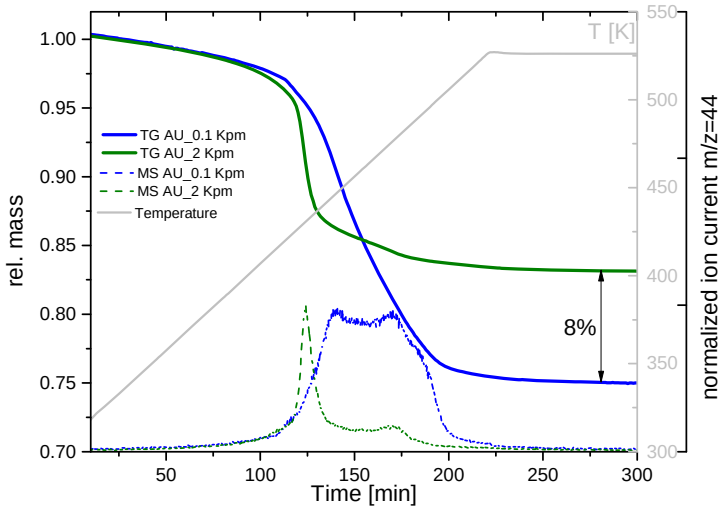

Figure 7: TG-MS measurement of the reduction of calcined precursors in 5%H_2 in Ar, 1Kpm. After reduction the catalyst is free of carabonates.

After reduction, Cu-SAs were measured by N_2O-RFC and varied in a range of 18–22 $m^2/\ g_{calc}^{-1}$ and 13–19 $m^2/\ g_{calc}^{-1}$ for the AU-red and ZM-red sample series, respectively (see Table 2). There was no unique relationship of the Cu-SA with the heating ramp of the samples, but it seemed there was a weak trend pointing to a lower surface area for the samples with higher HT-CO_3 content and lower heating ramp. One might expect a different behaviour, e.g. samples with a smaller crystallite domain size to yield a higher surface area. The fact that samples rich in HT-CO_3 show a smaller Cu-SA is a hint that there is a stronger embedment of the Cu particles in the slowly calcined samples. Additionally, this could also be a result of the higher dilution of the amount of Cu in the reactor by carbonate when loading it with a certain amount of calcined sample. However, this effect can only account for a fraction of the trend, as the mass loss difference is only about 5 % between samples with highest and lowest heating rate, but the differences in Cu-SA are about 20-30 %. Anyway, the absence of a linear trend between HT-CO_3 content and Cu-SA points to the possibility that some carbonate is present as a three-dimensional phase of its own without any binding effect to other crystals and thus diluting the active mass, while only a smaller faction of HT-CO_3 affects the binding of the oxide components and leads to embedding of copper.

Table 2: N_2O- and BET surface areas of calcination series AU and ZM calcined at different heating rates and BET surface areas of the precursors.

	AU		**ZM**	
	Cu-SA_{N2O} $[m^2\ g_{calc}^{-1}]$	**BET-SA** $[m^2\ g_{calc}^{-1}]$	**Cu-SA_{N2O}** $[m^2\ g_{calc}^{-1}]$	**BET-SA** $[m^2\ g_{calc}^{-1}]$
Precursor		55		43
Heating rate [Kpm]				
0.1	18	30	15	58
0.2	19	60	13	51
0.5	21	80	16	58
1	22	98	19	68
2	21	60	18	82

3.5. Catalytic activity in methanol synthesis

Activity in methanol synthesis from a 6% CO / 8% CO_2 syngas mixture with hydrogen was measured at 30 bar and 503 K (see Figure 8). The ZM derived catalysts started showing a high activity of more than 300 µmol $min^{-1}\ g_{calc}^{-1}$ in methanol synthesis. AU derived catalysts started with lower activities between 260 and 300 µmol $min^{-1}\ g_{calc}^{-1}$. As the more active ZM catalysts deactivated more rapidly, similar activity of both catalyst families was reached after 17 h TOS (time on stream). It is noted that in practical catalysis promoters such as Al_2O_3 are added to improve the stability of the Cu/ZnO catalysts. There was a weak apparent trend of the activity data (per mass of calcined precursor),

which showed that the samples with slower heating rate and thus more HT-CO_3 were less active, despite their lower crystallinity in the calcined state with smaller domain sizes of the oxides. A similar trend was already observed for the Cu-SA, although the relative differences in Cu-SA were bigger than the differences observed in activity. The higher activity of the ZM series at the very beginning of methanol synthesis is not easily explained, as the Cu-SA measured by N_2O-RFC was generally lower in the ZM compared to the AU series. This is another indicator that the Cu-SA_{N2O} is not a precise parameter for the activity in methanol synthesis when comparing different catalyst families [33].

Normalization of the activity to the mass of the reduced catalyst leads to alignment of the values in the series aurichalcite derived samples to the (see Figure S4) 260 µmol/$g_{reduced}$/min. These have been obtained under the assumption that the HT-CO_3 decomposes upon reduction of CuO during the catalyst's activation as it was shown on figure 7 and demonstrated previously [34, 35]by accounting for the weight fraction of HT-CO_3 as determined by TGA (Fig. 3). As the samples contain different amounts of HT-CO_3, which is released during reduction, the reactor loading of reduced catalyst is slightly different for the samples calcined with different heating rates even if the same mass of calcined materials was used. Thus the absolute amount of high temperature carbonate within one calcination series has a minor effect on the reaction rate with respect to the copper content in the reduced catalyst.

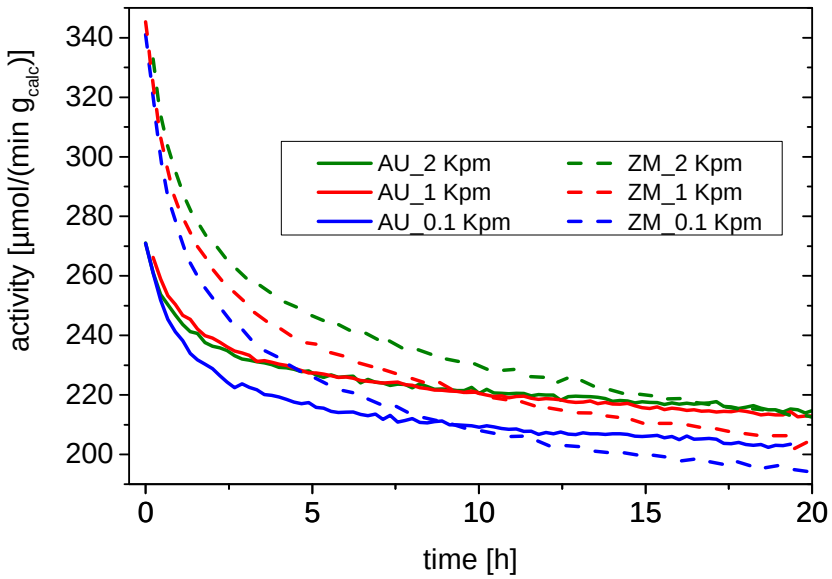

Figure 8: Activity of calcined at different heating rates AU (solid line) and ZM (dotted line) in methanol synthesis at 503 K and 30 bar.

The studied samples showed very close values of activities as for the abundance of reduced copper. Hence for the analysis of the catalytic relevance of the HT-CO_3 deactivation parameters has been chosen. For a comparison of the deactivation behaviour of the different catalysts, the relative activities $a_{rel}(t)=a(t)/a(0)$ were fitted with a simple Power-Law-Model according to $da_{rel}/dt = -k \cdot a^n$ as it was done in the literature previously [1, 36, 37]. Different deactivation orders n had to be used for the different catalyst families to result in a reasonable fit quality. A high order n=23 was used for the AU catalyst series, reflecting the fact that they show a strong deactivation at the beginning which levels off very quickly to show steady state values with only minor deactivation. It is worth noting that the calcined sample derived from Aurichacite precursor without high temperature carbonate exhibits much faster deactivation when tested as catalyst. The deactivation profile has most reliable fit with n=2 and k=0.23 (Fig S5). The exponent n is considered as to be related with metal particle growth. An exponent n of 2 has been ascribed to fundamentally different growth mechanism such as Ostwald ripening and particle migration coalescence [38]. The value of exponent n depends on the mobility of the crystallites on the support and upon the rate of merging of two colliding particles into a single particle. The modelling of crystallite sintering during heat treatment of supported metal catalyst was elaborately performed by E. Rodenstein and B. Pulvermacher [39]. In this original work the authors showed the exponent n is 4 or larger for sufficiently low particles mobilities and is lower than 3 for large surface mobility of particles. The exponent n is related to the size dependence of diffusion coefficients (diffusion controlled decay) or on rate constant of the particle merging process (sintering controlled decay). Diffusion control (n>4) is associated with strong metal-support interaction, but in sintering control (n<3) the interactions between the metal and the support is weaker. The ZM derived samples were fitted with lower reaction order values of n=9 which are of the order of previously used deactivation orders for deactivation processes explained by general sintering [1]. The faster deactivation of ZM derived samples during the 20 hours TOS can be explained by a less efficient separation of the Cu particles by ZnO due to the lower content of ZnO in the ZM samples acting to some extent as a physical spacer between the Cu particles formed during the reduction compared to the AU samples. Table 3 summarizes the deactivation constants for catalyst issued from the calcined precursor.

Table 3: Rate constants h^{-1} of deactivation fit using a simple Power-Law-Model (PLM).

Heating rate	AU (order: 23; R^2>0.92)	HT-CO3 in calcined sample / %	ZM (order: 9; R^2 >0.99)	HT-CO3 in calcined sample / %
2 Kpm	0.39	3	0.23	3
1 Kpm	0.28	6	0.45	4
0.5 Kpm	0.23	-		-
0.2 Kpm	0.92	-		-
0.1 Kpm	1.18	8	0.61	8

Within the ZM family it is observed, that the deactivation rate constants increase with increasing HT-CO_3 content in the calcined state. For the AU catalyst family the smallest deactivation rate constant is observed for intermediate HT-CO_3 content and moderate heating rates of the calcination step, with the by far largest deactivation rate constants for the samples which were prepared using the slowest heating rate during calcination. The initial turnover frequencies (TOF) under conditions applied are $9.1*10^{-3}$ s^{-1} for the HT-CO_3 free sample and $8.5*10^{-3}$ s^{-1} for the sample with 3% of residual high temperature carbonate. These values are in an excellent agreement with the data reported lately for Cu/ZnO/Al_2O_3 catalyst [40]. Despite very close start values of the turnover frequencies and activities (240 and 260 $\mu mol_{MeOH}/min/g_{calc}$ respectively) the deactivation behaviour of these samples exhibits dramatic difference. Fujita et al. [41] studied the variation of TOF for methanol synthesis with the dispersion CuO and ZnO in calcined samples and with Cu crystallite size in the reduced catalyst at a given Cu/Zn ratios. However TOF is not simply dependent on the copper crystallite size but varies with the Cu/Zn ratio. We believe that that rapid deactivation of carbonate free AU catalyst might be caused by the formation of CuO and ZnO aggregates during the calcination (Table S1), which predetermine broader Cu metal particle size distribution along with lower ZnO dispersion in the reduced catalyst. Although the increased absolute amount of the HT-CO_3 within one catalyst family does not improve the stability (Table 3) but the absence of carbonate species results in more severely pronounced activity decay (Fig S5.). The role of differently coordinated carbonate species in the calcined samples on the catalytic behaviour of the final catalyst could not be trivially explored, since it has a less influence than copper content or total amount of carbonates. It is observes that calcined ZM sample has no coordinated carbonate, whereas calcine AU sample contains monodentate coordinated species. On the other hand the copper content for AU is twice less as for ZM. As mentioned before the role of coordinated species might be consider as a binder between oxide components which affects the embedding of copper, but the free species have not any binding effect and act more likely as diluent. Thus, different parameters control the stability of the microstructure: (i) the amount and (ii) the distribution of the ZnO component. Both are influenced by the selection of the precursor phase. Additionally, the choice of the calcination conditions and the resulting HT-CO_3 phase likely influence the distribution of ZnO in the catalyst.

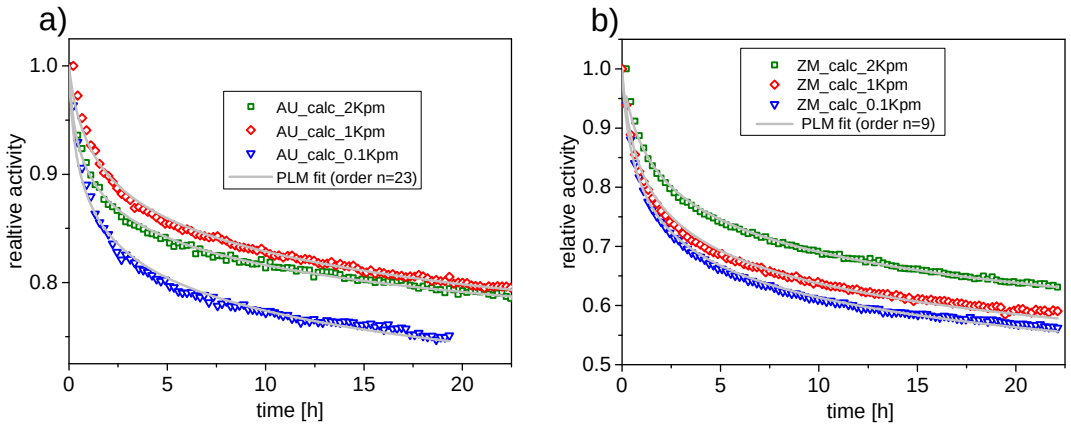

Figure 9. Relative activity $a_{rel}(t)=a(t)/a(0)$ and fits with Power-Law-Model $a_{rel}(t)=((n-1)k*t+1)^{-1/(n-1)}$. ZM derived samples deactivate faster due to sintering [1].

To illustrate the long term deactivation dynamics of the catalysts the curves were extrapolated to 450 days TOS and compared with the recent literature results. There is an agreement of the processed data with the deactivation profiles of Fichtl et al. [36] and Prieto et al. [37] on the long term scale. However the discrepancies are significantly pronounced during the first 250 hours TOS (Fig 10). The supported CuZn on SBA [37] catalysts undergo most rapid deactivation while the AU based catalysts tend to deactivate slower. The studied by Fichtl et al. a highly active catalysts named FHI Standard [34] and other ZM derived catalyst have close relative loss of activity however the initial loss is considerably slower for the Al promoted FHI standard [42].

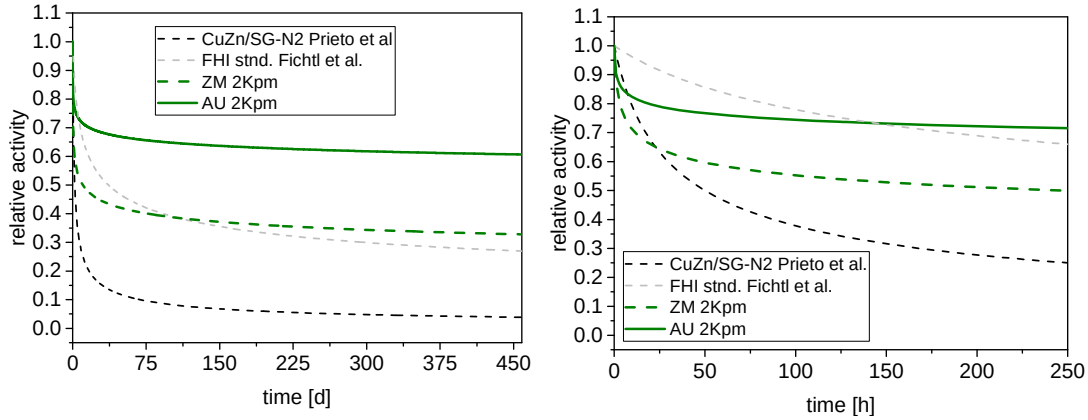

Figure 10. Extrapolated relative activities of the selected models. The AU derived samples exhibit slower deactivation during the first 1-3 days as compared with ZM.

The comparison however must be performed with great care since the reaction and altering conditions are not identical. The observed reaction rate constant depends strongly on feed and process conditions. For deeper insights into the deactivation dynamics of the catalyst of different

families more detailed microstructural analysis of the deactivated and altered catalyst is required as well as implementation of complementary techniques. Very convincing approaches for investigating the deactivation mechanisms of CO/CO_2 hydrogenation catalysts were nicely demonstrated by Rostrup-Nielsen et al. [43] and Fichtl et al. [36]. However this intriguing task remains beyond the extent of the present work.

4. Conclusion

By varying the heating ramp during calcination, the amount of HT-CO_3 was adjusted in calcined CuO/ZnO materials prepared from both binary ZM and AU precursors. Presence of large amounts of HT-CO_3 indicated that no significant segregation and crystallization of CuO and ZnO took place as shown with XRD. This observation is in line with previous reports associating the HT-CO_3 with a large Cu/Zn interface [2, 10]. Residual carbonates after calcination can affect the microstructure and defectivity of the final Cu particles by kinetic hindrance of their crystallization during the reduction. Presence of the carbonates in the calcined samples preserves high dispersion of strained Cu metal particles stabilized by ZnO nanoparticles in the reduced catalyst. Distinct changes in crystallinity, decomposition profile and IR absorption were observed. The differences of the catalytic activity in methanol synthesis did not reveal a beneficial effect of a high HT-CO_3 content. On the contrary, dilution of the active Cu by carbonate led to a small decrease of activity in methanol synthesis per g of calcined precursor. On the other hand, intermediate amounts of HT-CO_3 seem to result in improved stability and a smaller deactivation constant for the AU catalyst. Due to different deactivation behaviour the different precursor phases AU and ZM yielded catalysts with similar activities in methanol synthesis after 17 h TOS. ZM derived catalysts started with a higher activity, but exhibit a faster deactivation. However extrapolation plot of the activity data for longer TOS demonstrates similar absolute values of methanol production rates. The different deactivation behaviour of the ZM and AU can be related to different amounts of Cu in the samples, and a higher effectiveness of the ZnO spacer in the Zn-richer AU derived catalysts. Additionally the coordination of carbonate species, which were identified by IR measurements in the calcined precursors might affect the interdispersion of ZnO and CuO and could exert an implicit impact over the deactivation behaviour.

5. Acknowledgement

The authors thank Jasmin Allan for XRD and TG measurements and Maike Hashagen for BET measurements.

6. References

[1] J.B. Hansen, P.E.H. Nielsen, in: G. Ertl, H. Knözinger, F. Schüth, J. Weitkamp (Eds.), Handbook of Heterogeneous Catalysis, Wiley-VCH, Weinheim, 2008, pp. 2920-2944.

[2] B. Bems, M. Schur, A. Dassenoy, H. Junkes, D. Herein, R. Schlögl, Chem. Eur. J. 9 (2003) 2039-2052.

[3] C. Baltes, S. Vukojevic, F. Schüth, J. Catal. 258 (2008) 334-344

[4] G.J. Millar, I.H. Holm, P.J.R. Uwins, J. Drennan, J. Chem. Soc., Faraday Trans. 94 (1998) 593-600.

[5] D. Waller, D. Stirling, F.S. Stone, M.S. Spencer, Faraday Discussions of the Chemical Society 87 (1989) 107-120.

[6] P. Kowalik, M. Konkol, K. Antoniak, W. Próchniak, P. Wiercioch, J. Mol. Catal. A: Chem. 392 (2014) 127-133.

[7] M. Behrens, S. Zander, P. Kurr, N. Jacobsen, J. Senker, G. Koch, T. Ressler, R.W. Fischer, R. Schlögl, J. Am. Chem. Soc. 135 (2013) 6061-6068.

[8] M. Behrens, R. Schlögl, Z. anorg. allg. Chem. 639 (2013) 2683-2695.

[9] S. Fujita, S. Moribe, Y. Kanamori, M. Kakudate, N. Takezawa, Appl. Catal., A 207 (2001) 121-128.

[10] M. Schur, B. Bems, A. Dassenoy, I. Kassatkine, J. Urban, H. Wilmes, O. Hinrichsen, M. Muhler, R. Schlögl, Angewandte Chemie International Edition 42 (2003) 3815-3817.

[11] N. Koga, J.M. Criado, H. Tanaka, Thermochim. Acta 341 (1999) 387-394.

[12] A. Tarasov, J. Schumann, F. Girgsdies, N. Thomas, M. Behrens, Thermochimica Acta 591 (2014) 1-9.

[13] S. Fujita, S. Moribe, Y. Kanamori, N. Takezawa, React. Kinet. Catal. Lett. 70 (2000) 11-16

[14] M. Behrens, J. Catal. 267 (2009) 24-29.

[15] A. Coelho, TOPAS, 4.2 ed., Bruker AXS GmbH, Karlsruhe, Germany, 2003-2009.

[16] I. Arkhangelsky, A. Dunaev, I. Makarenko, N. Tikhonov, S. Belyaev, A. Tarasov, Non-Isothermal Kinetic Methods, Edition Open Access, Berlin, 2013.

[17] J. Opfermann, J. Therm. Anal. Calorim. 60 (2000) 641-658.

[18] S. Brunauer, P.H. Emmett, E. Teller, J. Am. Chem. Soc. 60 (1938) 309--319.

[19] E.P. Barrett, L.G. Joyner, P.P. Halenda, J. Am. Chem. Soc. 73 (1951) 373--380.

[20] G.C. Chinchen, C.M. Hay, H.D. Vandervell, K.C. Waugh, J. Catal. 103 (1987) 79-86.

[21] N.A. Tikhonov, I.V. Arkhangelsky, S.S. Belyaev, A.T. Matveev, Thermochim. Acta 486 (2009) 66-70.

[22] W. Busser, On the rate controlled reduction and calcination of methanol synthesis catalysts, Personal Communication, Personal Communication ed., 2006.

[23] H. Ruland, W. Busser, H. Otto, M. Muhler, Chemie Ingenieur Technik 86 (2014) 1890-1893.

[24] M. Reading, D. Dollimore, Thermochim. Acta (1994) 117-127.

[25] M. Behrens, F. Girgsdies, A. Trunschke, R. Schlögl, Eur. J. Inorg. Chem. 2009 (2009) 1347-1357.

[26] J.A. Goldsmith, S.D. Ross, Spectrochimica Acta Part A: Molecular Spectroscopy 24 (1968) 2131-2137.

[27] A.A. Khassin, H. Jobic, G.A. Filonenko, E.V. Dokuchits, A.V. Khasin, T.P. Minyukova, N.V. Shtertser, L.M. Plyasova, T.M. Yurieva, Journal of Molecular Catalysis A: Chemical 373 (2013) 151-160.

[28] I. Melián-Cabrera, M. López Granados, J.L.G. Fierro, Physical Chemistry Chemical Physics 4 (2002) 3122-3127.

[29] B. Reddy, R. Frost, A. Locke, Transition Met. Chem. 33 (2008) 331-339.

[30] K.I. Hadjiivanov, G.N. Vayssilov, Adv. Catal. 47 (2002) 307-511.

[31] M. Schmidt, H. Lutz, Phys. Chem. Miner. 20 (1993) 27-32.
[32] K. Föttinger, R. Schlögl, G. Rupprechter, Chem. Commun. (2008) 320-322.
[33] O. Martin, J. Pérez-Ramírez, Catalysis Science & Technology 3 (2013) 3343.
[34] J. Schumann, T. Lunkenbein, A. Tarasov, N. Thomas, R. Schlögl, M. Behrens, ChemCatChem 6 (2014) 2889-2897.
[35] A. Tarasov, S. Kühl, J. Schumann, M. Behrens, High Temperatures-High Pressures 42 (2013) 377-386.
[36] M.B. Fichtl, D. Schlereth, N. Jacobsen, I. Kasatkin, J. Schumann, M. Behrens, R. Schlögl, O. Hinrichsen, Applied Catalysis A: General 502 (2015) 262-270.
[37] G. Prieto, J.D. Meeldijk, K.P. de Jong, P.E. de Jongh, Journal of Catalysis 303 (2013) 31-40.
[38] A.K. Datye, Q. Xu, K.C. Kharas, J.M. McCarty, Catalysis Today 111 (2006) 59-67.
[39] E. Ruckenstein, B. Pulvermacher, AlChE J. 19 (1973) 356-364.
[40] F. Studt, M. Behrens, E.L. Kunkes, N. Thomas, S. Zander, A. Tarasov, J. Schumann, E. Frei, J.B. Varley, F. Abild-Pedersen, J.K. Nørskov, R. Schlögl, ChemCatChem 7 (2015) 1105-1111.
[41] S. Fujita, K. Yoshinori, M.S. Agus, T. Nobutsune, Catalysis Today 45 (1998) 241-244.
[42] M. Behrens, S. Zander, P. Kurr, N. Jacobsen, J. Senker, G. Koch, T. Ressler, R.W. Fischer, R. Schlogl, Journal of the American Chemical Society 135 (2013) 6061-6068.
[43] J.R. Rostrup-Nielsen, K. Pedersen, J. Sehested, Applied Catalysis A: General 330 (2007) 134-138.